Mon. Not. R. Astron. Soc. **000**, 1–17 (2003) Printed 2 February 2008 (MN LATEX style file v2.2)

Galaxy evolution in clusters up to $z = 1.0^{\star}$

S. Andreon,[1]†, J. Willis[2] ‡, H. Quintana[2], I. Valtchanov[3]§, M. Pierre[3] and F. Pacaud[3]
[1] *INAF–Osservatorio Astronomico di Brera, Milano, Italy*
[2] *Departamento de Astronomía y Astrofísica, Pontificia Universidad Católica de Chile, Santiago, Chile*
[3] *CEA/DSM/DAPNIA, Service d'Astrophysique, Gif-sur-Yvette, France*

Accepted ... Received ...

ABSTRACT

We present a combined study of the colour–magnitude relation, colour distribution and luminosity function of a sample of 24 clusters at redshifts $0.3 < z < 1$. The sample is largely composed of X–ray selected/detected clusters. Most of the clusters at redshifts $z < 0.6$ display X–ray luminosity or richness typical of poor clusters or groups, rather than the more typical, massive clusters studied in literature at redshifts $z \gtrsim 0.3$. All our clusters, including groups, display a colour–magnitude relation consistent with a passively evolving stellar population formed at a redshift $z_f \gtrsim 2$, in accordance with observed galaxy populations in more massive clusters studied at comparable redshifts. Colours and luminosity functions show that the cluster galaxy population is consistent with the presence of at least two components: old systems formed at high redshift that have evolved passively from that epoch, together with a galaxy population displaying more recent star formation. The former population forms at $2 \lesssim z_f \lesssim 5$, the latter at redshifts $z < 1$. A model in which stars do not evolve is clearly rejected by both by the colour of reddest galaxies and by the characteristic luminosity m^* measures. All clusters (with one possible exception) are detected independently by an almost three dimensional optical search employing sky position and colour – this despite the primary X–ray selection and low X–ray flux/optical richness displayed by the majority of the sample.

Key words: Galaxies: evolution — galaxies: clusters: general — galaxies: luminosity function – galaxies: clusters: individual: F1557.19TC, RX J0152.7-1357, VMF98 34, VMF98 40, VMF98 43, XLSSC 001, XLSSC 002, XLSSC 003, XLSSC 004, XLSSC 005, XLSSC 006, XLSSC 007, XLSSC 008, XLSSC 009, XLSSC 010, XLSSC 012, XLSSC 013, XLSSC 014, XLSSC 016, XLSSC 017, XLSSC 018, XLSSC 019, XLSSC 020, RzCS 001

1 INTRODUCTION

The colour–magnitude relation and the luminosity function (LF) provide quantitative measures of galaxy evolution. The colour–magnitude relation, also known as the red sequence, is a general observed characteristic of galaxies in clusters (e.g. Garilli et al. 1996, Stanford, Eisenhardt & Dickinson 1998). The homogeneity in colour of galaxies on the red sequence, both observed across a range of clusters (Ellis et al. 1997; Andreon 2003a,c) and within individual systems (e.g. Bower et al. 1992, Stanford et al. 1998), and the apparent passive evolution of cluster elliptical galaxies (Kodama & Arimoto 1997, Stanford et al. 1998; Kodama et al. 1998), all imply that the luminosity–weighted stellar populations within such galaxies are uniformly old ($z_f \gtrsim 2$).

The colour–magnitude relation constrains the evolution of the reddest cluster galaxies whereas the LF describes the spatial density per unit luminosity interval and its evolution provides an overall measure of the changing cluster galaxy population. The local ($z < 0.3$) cluster galaxy LF has been derived for large numbers of systems (Garilli, Maccagni & Andreon 1999; Paolillo et al. 2001; de Propris et al. 2003) and the evolution of the LF at increasing redshift (Andreon 2004) is consistent with predictions based upon passive stellar evolution. Near infra–red (NIR; in this case K–band) observations have confirmed that the mean cluster galaxy LF

⋆ Based on observations obtained at ESO and Cerro–Tololo telescopes.
† email: andreon@brera.mi.astro.it
‡ Present Address: Department of Physics and Astronomy, University of Victoria, Victoria, Canada
§ Present Address: Imperial College, London, UK

Table 1. Summary of the cluster sample considered in this paper.

Name	Colour detected?	Optical centre (J2000) RA	DEC	z	Filters	Notes
XLSSC 008	–	02 25 20.2	-03 48 30	0.297	I	
XLSSC 013	Y	02 27 25.9	-04 32 15	0.307	Rz'	
XLSSC 018	Y	02 24 01.6	-05 05 25	0.322	Rz'	
XLSSC 009	–	02 26 44.7	-03 41 02	0.327	I	
XLSSC 010	–	02 27 22.3	-03 21 41	0.329	I	
XLSSC 016	Y	02 28 28.2	-04 59 46	0.332	Rz'	
XLSSC 014	Y	02 26 34.5	-04 03 55	0.344	Rz'	
XLSSC 017	Y	02 26 27.4	-04 59 55	0.381	Rz'	blended with XLSSC 020
VMF98 34	Y	03 41 57.0	-45 00 11	0.408	Rz'	X–ray selected
XLSSC 006	Y	02 21 45.8	-03 46 08	0.429	RIz'	
XLSSC 012	Y	02 28 27.4	-04 25 48	0.433	Rz'	
VMF98 43	Y	05 29 38.0	-58 48 20	0.466	Rz'	X–ray selected
RzCS 001	Y	02 24 04.3	-05 17 22	0.494	RIz'	colour selected, X–ray undetected
XLSSC 019	Y	02 24 11.8	-05 22 47	0.494	Rz'	
XLSSC 020	Y	02 26 32.8	-05 00 32	0.494	Rz'	blended with XLSSC 017
Cl0412	Y	04 12 49.9	-65 50 44	0.51	Rz'	optically selected, alias F1557.19TC
XLSSC 007	N	02 24 09.0	-03 55 09	0.557	RIz'	dubious X–ray-optical identification
VMF98 40	Y	05 21 12.0	-25 31 13	0.581	Rz'	X–ray selected
XLSSC 001	–	02 24 57.1	-03 48 53	0.614	I	
XLSSC 002	–	02 25 32.5	-03 55 10	0.772	I	
RXJ0152	Y	01 52 43.9	-13 57 19	0.831	Rz'	X–ray selected, alias RX J0152.7-1357
XLSSC 003	–	02 27 37.6	-03 18 07	0.838	I	
XLSSC 004	Y	02 25 28.4	-05 06 57	0.88	RIz'	
XLSSC 005	Y	02 27 09.7	-04 18 05	1.0	RIz'	high z structure

Notes: redshift for XLSSC clusters are taken from Valtchanov et al. (2003) & Willis et al. (2004). VMF98 34, VMF98 40 and VMF98 43, are drawn from the 160 deg^2 survey (Vikhlinin et al. 1998, Mullis et al. 2002), while RXJ0152 is drawn from the SHARC survey (Romer et al. 2000), and also detected in the WARPS survey (Ebeling et al. 2000). Cl0412 is an optically selected cluster (Couch et al. 1991) later observed (and detected) in X–ray (Smail et al. 1997).

continues to evolve passively to redshift unity (de Propris et al. 1999). NIR fluxes received from galaxies at redshifts $z < 1$ are dominated by rest–frame emission arising from stellar types G and later. Therefore, although the NIR cluster galaxy LF provides a suitable measure of the passive evolution of stellar mass contained in such systems, the LF computed from red optical passbands (i.e. sampling rest–frame blue emission) provides a more sensitive measure of active luminosity evolution, i.e. secondary star formation events.

Current measures of the optical LF evolution of cluster galaxies at $z > 0.3$ are few (Nelson et al. 2001; Barrientos & Lilly 2003). The present paper addresses this issue and combines a discussion of LF evolution in cluster galaxies with a simultaneous assessment of the colour–magnitude relation. Data acquisition and reduction is discussed in Section 2. Section 3 presents the colour–magnitude relation, colour distribution and the LF computed for individual clusters. Section 3 also discusses the evolution of the above quantities with redshift. The main results are presented and discussed in Section 4, i.e. we demonstrate that the cluster galaxy population is consistent with the presence of at least two components: old systems formed at high redshift that have evolved passively from that epoch, together with a galaxy population displaying more recent star formation. We discuss constraints placed on the evolution of both populations by the current data set.

Throughout this paper we assume a Friedmann–Robertson–Walker–Lemaitre cosmological model described by the parameters $\Omega_M = 0.3$, $\Omega_\Lambda = 0.7$ and $H_0 = 70$ kms^{-1} Mpc^{-1}.

2 THE CLUSTER SAMPLE: OBSERVATIONS, DATA REDUCTION AND COLOUR ANALYSIS

2.1 The cluster sample

The cluster sample presented in this paper is drawn from a number of sources and represents a heterogeneous data set. Uniform photometry was obtained for all clusters and details are presented in Table 1. Eighteen clusters were observed as part of the X–ray Multi–Mirror (XMM) Large Scale Structure (LSS) survey (Pierre et al. 2004) which aims to determine the large scale structure of the Universe as traced by galaxy clusters[1]. An additional 5 clusters were added to this sample from the literature. The majority of the clusters are drawn from X–ray selected samples; two (RzCS 001 & Cl0412) are optically selected, the latter being later X–ray detected. The nature of the most distant cluster, XLSSC 005, is ambiguous (Valtchanov et al. 2004). Although the system displays extended X–ray emission and a concentration of galaxies in redshift space, there are several other galaxies in the cluster surroundings ($0.92 < z < 1.05$),

[1] The XMM–LSS survey area is centred on the coordinates $\alpha = 02:18:00$, $\delta = -07:00:00$ (J2000).

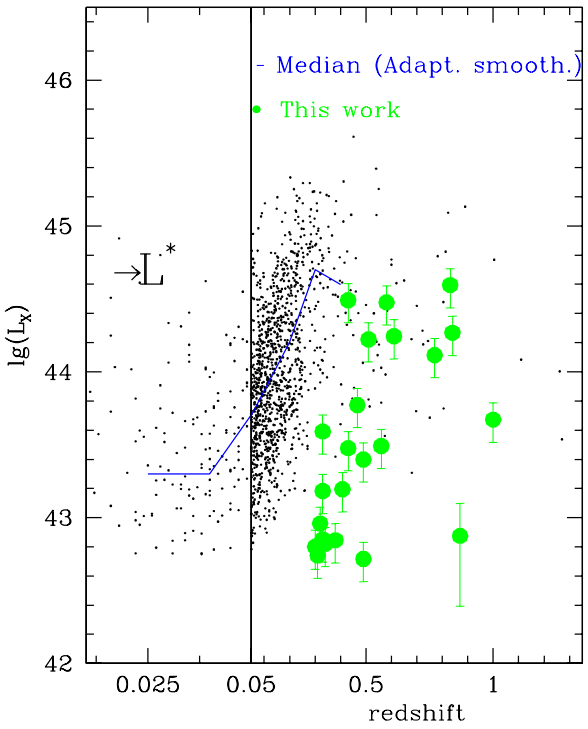

Figure 1. X-ray luminosity measured in the [0.1-2.4] keV rest–frame versus redshift for clusters drawn from literature (black dots) and XLSSC clusters (green circles with error bars). The blue curve is an adaptively smoothed running median of literature points.

suggesting perhaps a more complex structure. The redshift thickness of this structure is negligible, and therefore neglected within our subsequent analyses.

Figure 1 shows the X–ray luminosity in the [0.1-2.4] keV rest–frame band versus redshift for more than 1000 clusters in literature and listed in the X-Ray Galaxy Clusters Database (BAX, black dots), and for all X–ray detected clusters studied here (green circles with error bars). The horizontal arrow indicates the characteristic L_X^* luminosity reported by Ebeling et al. (1997). The curve is an adaptively smoothed running median of literature points. The X–ray luminosity of the clusters considered in this paper are typically lower than clusters presented in the literature (e.g., Mullis et al. 2003; Romer et al. 2000; Ellis et al. 1997) at similar redshift. In particular, at redshifts $z < 0.6$, XLSSC clusters have X–ray luminosities characteristic of low mass clusters and groups (Willis et al. 2004). This is expected, given the present area coverage and limiting flux of the XMM–LSS project (Pierre et al. 2004).

All clusters presented in this paper (including the complex structure XLSSC 005) have at least two concordant redshifts in addition to the presence of an unambiguous galaxy overdensity in multi–colour CCD images. We note that, though cluster XLSSC 007 is confirmed spectroscopically (Willis et al. 2004) with at least 10 members, there exists a large (1.2 arcminute) offset between the optical galaxy overdensity and the centroid of the X–ray emission. Though the optical cluster is clearly real, the X–ray flux for XLSSC 007 will be greatly overestimated should the observed X–ray emission arise from a second cluster along the line of sight.

2.2 Observations and data reduction

All clusters presented in this paper have been observed in R, z and/or I passbands as detailed in Table 1. Optical R– and z'–band ($\lambda_c \sim 9000$Å) images were obtained at the Cerro Tololo Inter–American Observatory (CTIO) 4m Blanco telescope during two observing runs, in August 2000 and November 2001, with the Mosaic II camera. Mosaic II is a 8k×8k camera with a 36×36 arcminute field of view. Typical exposure times were 1200 seconds in R and 2×750 seconds in z'. Seeing in the final images was between 1.0 and 1.4 arcseconds Full–Width at Half–Maximum (FWHM) in the November 2001 run (when all clusters except XLSSC 006 were observed), and 0.9 to 1.0 arcsec FWHM in the August 2000 run (XLSSC 006 observations). The useful nights of the two observing runs were photometric. Images were trimmed and bias corrected. A flat field correction was applied together with an illumination correction (where required) and interference fringes were removed from z'–band images. In the data reduction we employ the `FLIPS` software package (Cuillandre, in preparation). Where multiple exposures of the same field were available, cosmic rays were identified and images were combined. Extensive comparisons to Landolt (1992) standard stars, sky regions in the Early Data Release of the Sloan Digital Sky Survey (SDSS; Stoughton et al. 2002), and overlapping regions between pointings demonstrated that the photometric zero point is accurate to better 0.03 mag over the entire instrument field of view. A detailed description of these data reduction techniques will presented in a forthcoming paper presenting optically selected galaxy clusters within the XMM–LSS survey (Andreon et al. 2004).

Additional I–band images were obtained at the European Southern Observatory (ESO) 8.2m Very Large Telescope (VLT) facility employing the FOcal Reduction Spectrograph (FORS2) in September 2002 as part of pre–imaging of spectroscopic target fields. The FORS2 instrument consists of two 2k×4k CCDs with a field of view of 7×7 arcminutes. Exposure times were either 2×150 seconds or 4×150 seconds and observations were performed under photometric sky conditions. FORS2 images were reduced using standard techniques using IRAF[2]. Seeing in the final images were $0.6 - 0.9$ arcseconds FWHM.

Object magnitudes are quoted in the photometric system of the associated standard stars: R and I magnitudes are calibrated with Landolt (1992) stars, while z' magnitudes are calibrated with SDSS (Smith et al. 2002) standard stars. Source detection and characterization was performed employing SExtractor v2 (Bertin & Arnouts 1996). Colours are computed within a fixed 1.9 arcsecond radius aperture, whereas magnitudes are computed within an angular aperture of projected size equal to 15.3 kpc radius for objects at the cluster redshift.

[2] IRAF is distributed by the National Optical Astronomy Observatories, which are operated by the Association of Universities for Research in Astronomy, Inc., under cooperative agreement with the National Science Foundation.

A fixed angular aperture is employed to compute object colours, irrespective of the object redshift. We adopt this approach as only limited spectroscopic information is available within each cluster field. Employing a fixed angular aperture translates to a uniform metric aperture for all galaxies located at the cluster redshift. Colours computed within the adopted 1.9 arcsecond aperture are biased by differential seeing effects between the R– and z'–band images. A bias correction is applied employing bright stars located within each field. Several possible angular radii were considered, and 1.9 arcseconds was selected as a compromise figure that generated acceptable source signal–to–noise ratios together with a small correction for differential seeing effects. The median absolute correction (over all CTIO pointings) is 0.05 mag and the scatter is 0.05 mag.

A fixed metric aperture, corresponding to a radius of 15.3 kpc at each cluster redshift is employed to determine galaxy photometry for the LF computation. The particular aperture applicable to each cluster is also applied to galaxies within the control field. This metric aperture is employed in order to avoid introducing an unnecessary bias associated with the use of non–metric apertures (Dalcanton 1998) which can mimic the effect of redshift evolution in the LF. The value for the aperture radius, 15.3 kpc, permits a consistent comparison between the results of the current study and the LF derived for 65 low redshift ($z < 0.25$) clusters by Garilli, Maccagni & Andreon (1999 – hereafter GMA99), that adopt the same aperture when cast within their adopted cosmological model.

At faint magnitude limits, galaxies displaying low central surface brightness values are detected with rapidly decreasing frequency. Aperture magnitude completeness limits have been estimated according to the prescription of Garilli, Maccagni & Andreon (1999), Andreon et al. (2000), and Andreon & Cuillandre (2002), by considering the magnitude of the brightest galaxies displaying the lowest detected central surface brightness values. Only galaxies brighter than this completeness limit are considered in this paper.

Bright objects (typically $R < 22$, $z' < 22$), whose compactness computed using the SExtractor stellar classifier leads to a relatively unambiguous stellar classification, are discarded from the galaxy sample. Fainter stars are subtracted in a statistical manner following Andreon & Cuillandre (2002). The statistical nature of this approach avoids incorrectly excluding faint, compact galaxies from the sample. The control field used in the statistical subtraction procedure is separated from the science fields by no more than one degree and, as observations are performed at high Galactic latitudes, star counts within the control field are expected to reproduce those of the science fields.

2.3 Colour analysis and cluster detection

Galaxy clusters have been detected employing a method similar to the red sequence method of Gladders & Yee (2000). The method employed in this paper differs from the Gladders & Yee (2000) approach in several key areas, as described when it was applied (Andreon 2003a,b) to the SDSS Early Data Release (Stoughton et al. 2002). In summary, the method exploits the observed trend that the majority of galaxies in clusters display similar colours, while non–cluster galaxies located along the line–of–sight display considerable variation of observed colours, both because they are drawn from a larger interval of redshift and because the field galaxy population at a given redshift displays a larger variation in colour than a typical cluster galaxy population. The algorithm identifies local galaxy overdensities displaying similar $R - z'$ colours, and is considered at several angular scales. The applied colour filtering effectively removes most of the "background" galaxies (see Figure 3 and later discussion).

Only one cluster (XLSSC 007), of the 25 clusters studied here, is undetected at the $1 - 5 \times 10^{-6}$ confidence level. The remaining clusters present such sufficiently well–characterised detections that the optical images used to detect each cluster also permit detailed colour and LF studies.

3 RESULTS

3.1 The colour–magnitude distribution

Figure 2 displays colour magnitude diagrams constructed for clusters listed in Table 1 with R– and z'–band photometry. Two sample distributions are displayed: The first sample (open points) consists of galaxies brighter than the completeness limit (vertical dashed line) located within a specified radius from the cluster centre. This radius is specified to optimize the signal to noise ratio of the resulting LF computation. A radius of 2 arcminutes was adopted for the majority of the clusters. Exceptions to this value include clusters with a large projected extent (VMF98 34, VMF98 43, XLSSC 004, XLSSC 014, XLSSC 016, and XLSSC 020), for which a 3 arcminute radius was applied. In addition, a 1.5 arcminute radius was applied in two cases: XLSSC 017 – to reduce any contamination from the nearby cluster XLSSC 020; and XLSSC 007 – to reduce any effect from an unassociated foreground galaxy located 2 arcminutes from the cluster centre. The same set of apertures are employed to compute both the cluster colour distributions and the LFs. An angle of two arcminutes corresponds to a distance of $0.53, 0.80, 0.96$ Mpc when projected at redshifts $z = 0.3, 0.6, 1$ respectively.

The red sequence within each cluster is clearly apparent at redshifts $z < 0.6$, although a comparison of individual clusters demonstrates that their visual appearance varies considerably (e.g. XLSSC 006 compared to VMF98 43). The red sequence is sampled over an increasingly limited magnitude range with increasing redshift and is more heavely contaminated by background galaxies. However, the sequence remains clearly identifiable to redshifts $z = 0.84$.

The red envelope of the red sequence is defined by the reddest (i.e. larger colour value) horizontal line displayed in each sub–panel of Figure 2. The value of the red envelope is derived from the median colour of the three brightest galaxies considered to be viable cluster members, i.e. galaxies that are too blue or too bright to be plausibly at the cluster redshift are discarded.

The second sample of objects displayed in Figure 2 consists of a heterogeneous sample of galaxies with spectroscopic redshifts (Valtchanov et al. 2004; Willis et al. 2004; supplemented by NED and private communications for clusters drawn from literature), selected with no constraint with respect to z' magnitude or distance to the defined cluster centre. A galaxy is defined as a cluster member if lies within three σ_v of the centre of the cluster line–of–sight velocity distribution. Exceptions to this criterion are clusters lacking a

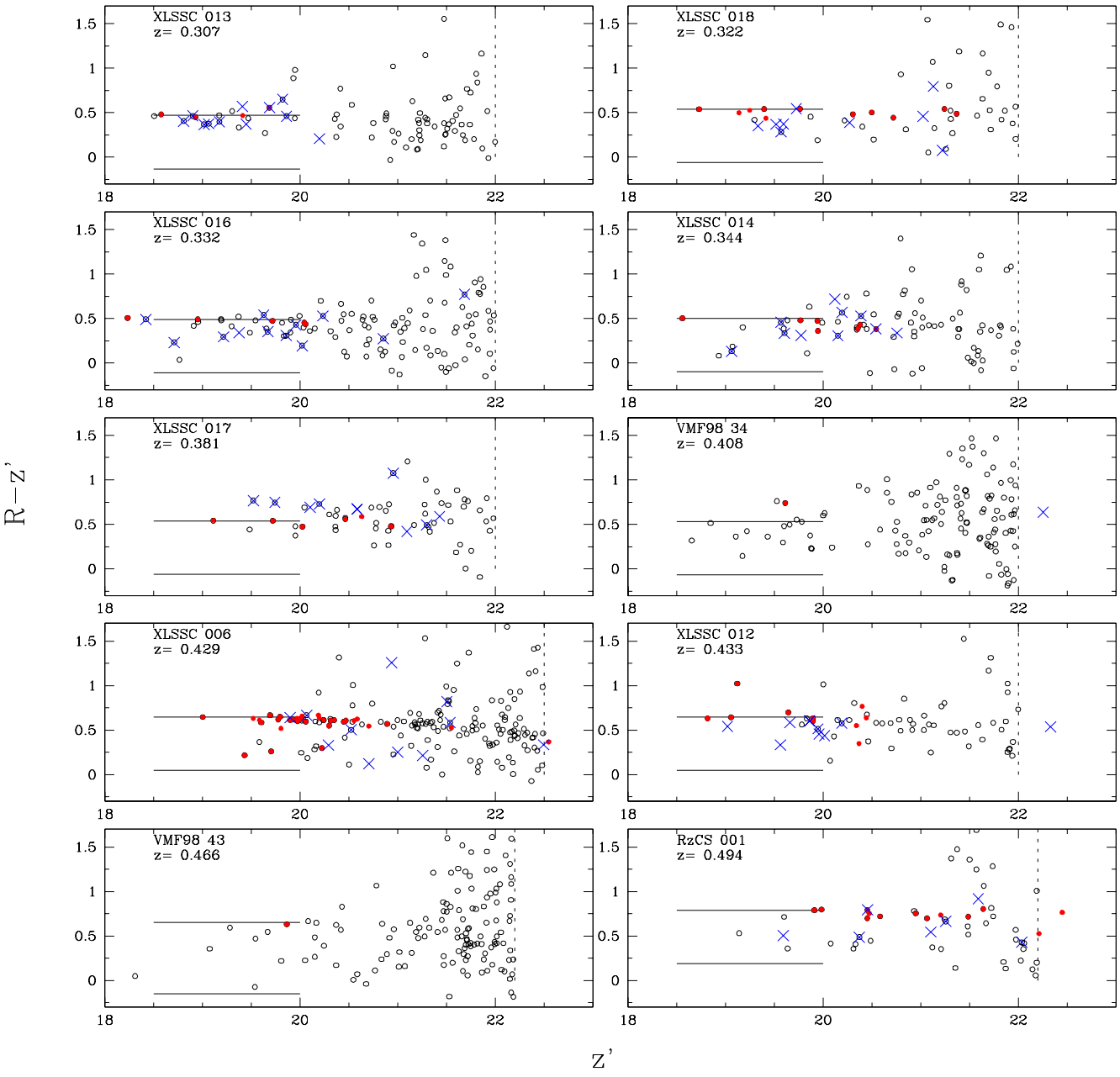

Figure 2. Colour–magnitude diagram for galaxies (open circles) brighter than the z' magnitude limit (vertical line). The horizontal lines indicate the colour range adopted for the LF derivation. Most of the spectroscopically confirmed members (red filled circles) are located within this colour range. Interlopers (blue crosses) are often located outside this colour range (e.g. XLSSC 004 or XLSSC 020). A small number of cluster members are scattered to colours significantly redder than this colour range, mainly as a result of source crowding and consequent deblending problems.

well–defined σ_v value (literature clusters and XLSSC 004), for which a value of $\sigma_v = 1000$ kms^{-1} is adopted. Galaxies with spectroscopic redshifts that do not satisfy this criterion are considered interlopers. Due to the complex nature of the system XLSSC 005, we do not include objects with spectroscopic redshifts in the discussion of this system. The distribution of spectroscopic cluster members (red points) coincides with and reinforces the colour–magnitude relation defined by the photometry alone.

3.2 Interpreting the colour distribution for each cluster

The colour distribution of galaxies brighter than the z'–band completeness limit within each cluster field is displayed in Figure 3. In each case, the colour distribution within the cluster radius defined in the previous section is compared to the colour distribution, normalized to the cluster area, of the whole MOSAIC II image (36 × 36 square arcminutes) in which the cluster is observed At redshifts $z \lesssim 0.8$, a significant excess of galaxies is observed toward the cluster field

Figure 2 – *continued*

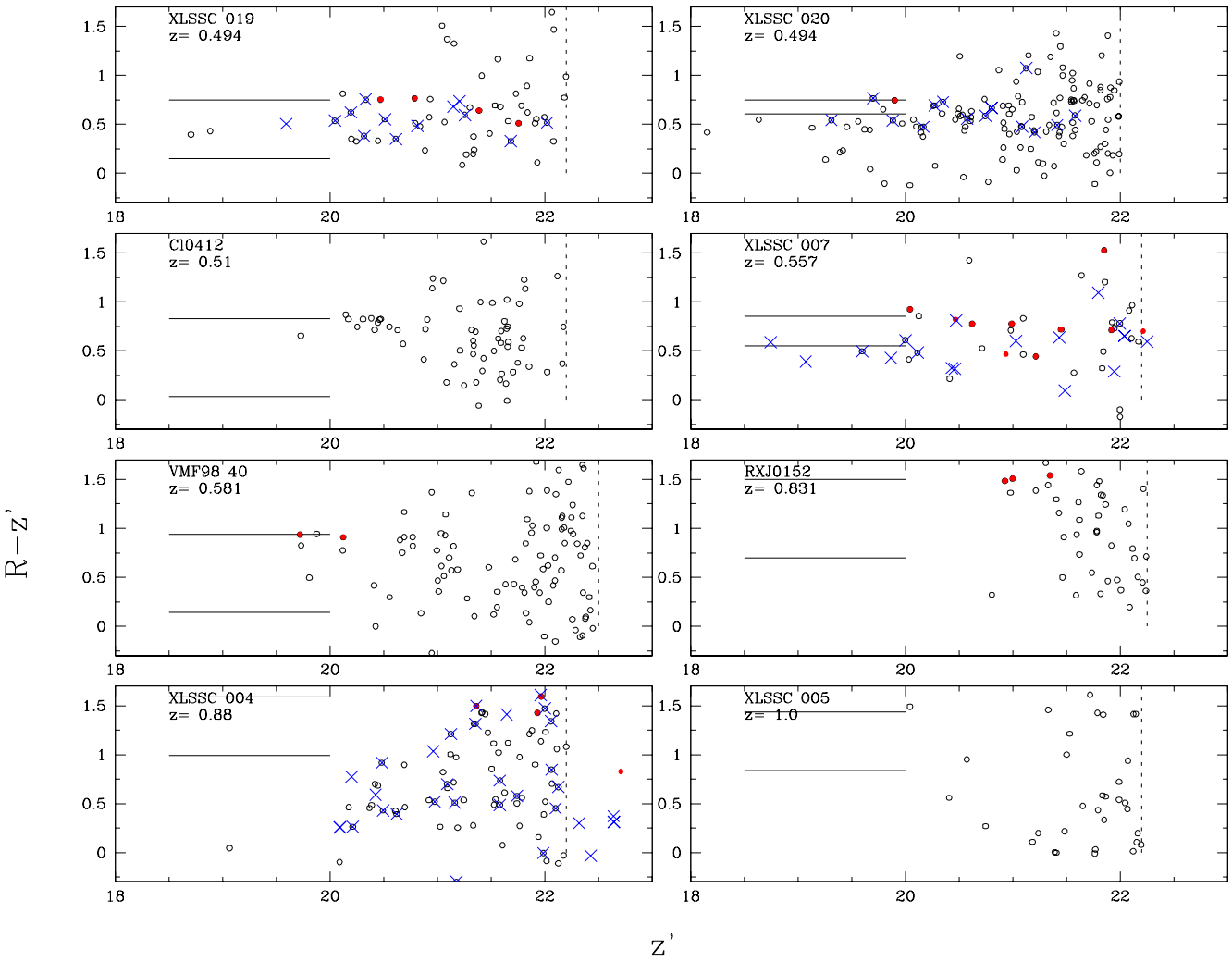

compared to the control field – whether computed over a specific colour interval or integrated over the entire colour distribution. The excess due to the cluster is sufficiently significant that clusters should be apparent as a spatial overdensity in a z'–band catalogue alone. At redshifts $z \gtrsim 0.8$, the excess of galaxies in colour space due to the cluster compared to the background is only significant within a limited (red) colour interval. These clusters are unlikely to be identified via a galaxy overdensity in a single photometric band, i.e. by neglecting the colour information. All clusters within the sample display a significant numerical excess over a limited colour interval (typically ± 0.3 mag), indicating that clusters may be identified effectively at redshifts $z \gtrsim 0.8$ by methods that employ colour selection to suppress background galaxy signals (Section 2.3). All clusters, with the exception of XLSSC 007, were in fact detected in a 3 dimensional space defined by sky position and $R-z'$ colour (Table 1).

A local ($z < 0.34$) cluster comparison sample, detected using a preliminary version of the same cluster detection algorithm used in this paper, is shown in Figure 1 of Andreon (2003a). The colour distribution of this local sample is qualitatively quite similar to the one shown in Figure 3. A detailed study of the evolution of the colour distribution (i.e. on the Butcher–Oemler effect) will be presented in a later study.

The cluster sample presented in this paper is predominantly X–ray selected/detected. The identification of a red sequence of galaxies associated with each cluster would initially seem at variance with Donahue et al. (2002), who claim that X–ray clusters presented in their survey do not all display a prominent red sequence. However, as the latter authors note and Gladders & Yee (2000) show, clusters do not require a prominent red sequence to be detected by a methods that search for overdensities of galaxies of similar (but not identical) colour. This refinement of the definition of the red sequence would appear to resolve the apparent contradiction between our finding and Donahue et al. (2002) claim and confirming the recent results by Gilbank, Bower, Castander, & Ziegler (2003), based on a low ($z < 0.4$) redshift sample.

The clusters presented in this paper display a range of masses (as determined by either dynamical or X–ray information, or both). In particular, XLSSC clusters at $z < 0.6$ display X–ray luminosities comparable to low richness clusters or groups (Figure 1). Therefore, the detection of galaxy

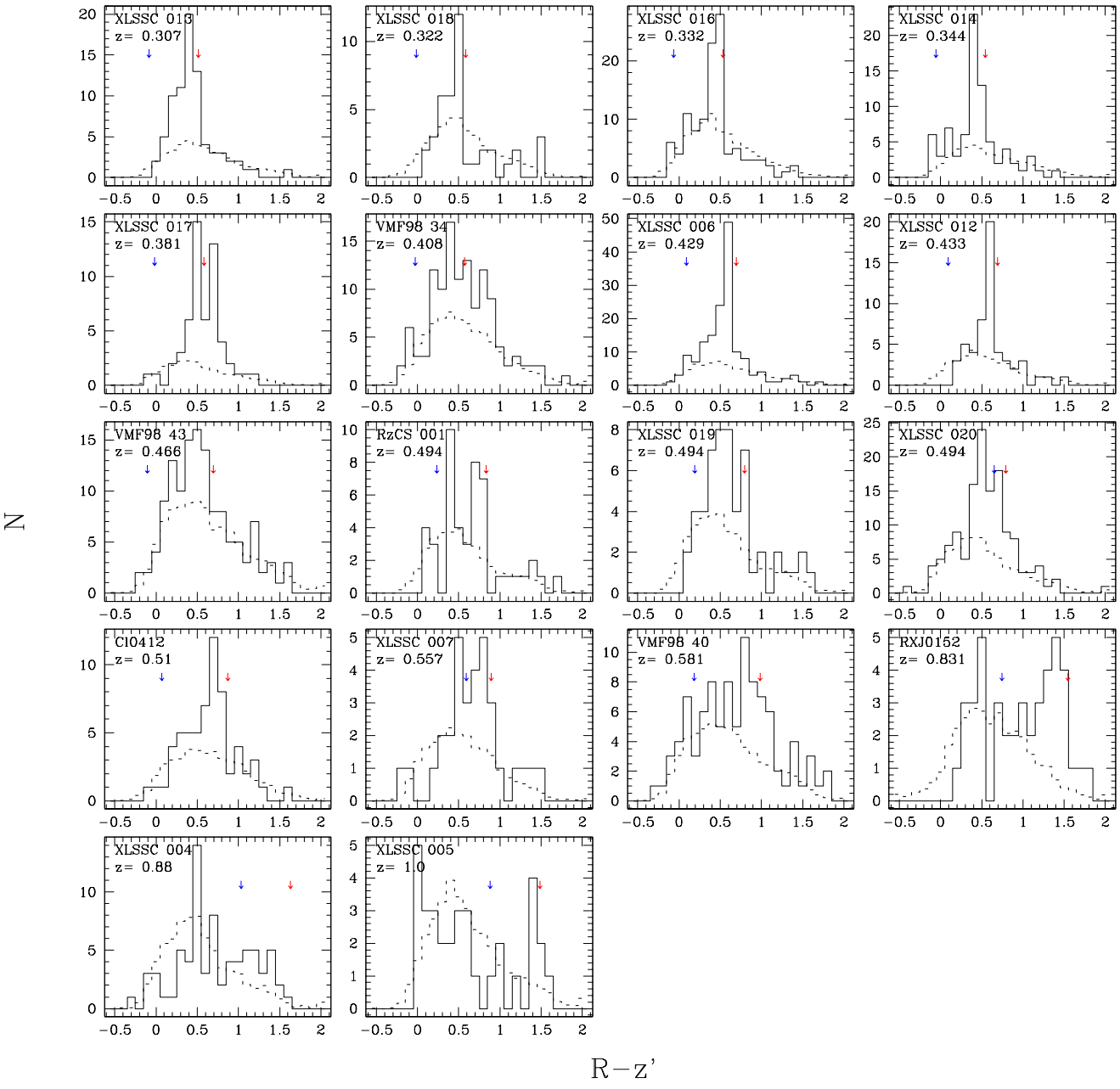

Figure 3. Colour histograms of galaxies brighter than the z' completeness magnitude limit in each cluster field. The solid histogram refers to the cluster field, while the dashed histogram indicates the colour distribution of the control field normalized to the cluster field area. The arrows mark the colour range adopted for the LF derivation. There is no statistically significant (at the 99.9995 % or greater confidence level) excess of galaxies outside this range, except in obvious cases (e.g. when another cluster is located along the line of sight).

overdensities in the 3–space defined by colour and sky location, at the location of extended X–ray sources indicates that such techniques may provide a promising route to confirm the nature of low mass X–ray selected clusters.

However, colour plus position selection alone does not constrain the extension in redshift of the identified structure. A filamentary structure of galaxies seen along the line of sight is, without spectroscopic data, hard to distinguish from a cluster and both scenarios can in principle give rise to the "cluster" detection. Spectroscopic observations of a sample of colour selected structures are therefore required to measure the frequency of each type of structure (clusters versus non–virialised large–scale structure). The spectroscopic cluster sample presented in this paper contains a colour selected cluster undetected in X–ray (RzCS 011). This system is confirmed spectroscopically and displays a well–defined mean redshift and distribution of rest–frame velocities. It is, therefore, a cluster in the sense of being a gravitationally bound systems of galaxies, altough undetected in X–rays. Therefore, colour selection techniques provide a method to identify clusters displaying a broad range of X–ray properties, possibly sampling the cluster mass function deeper

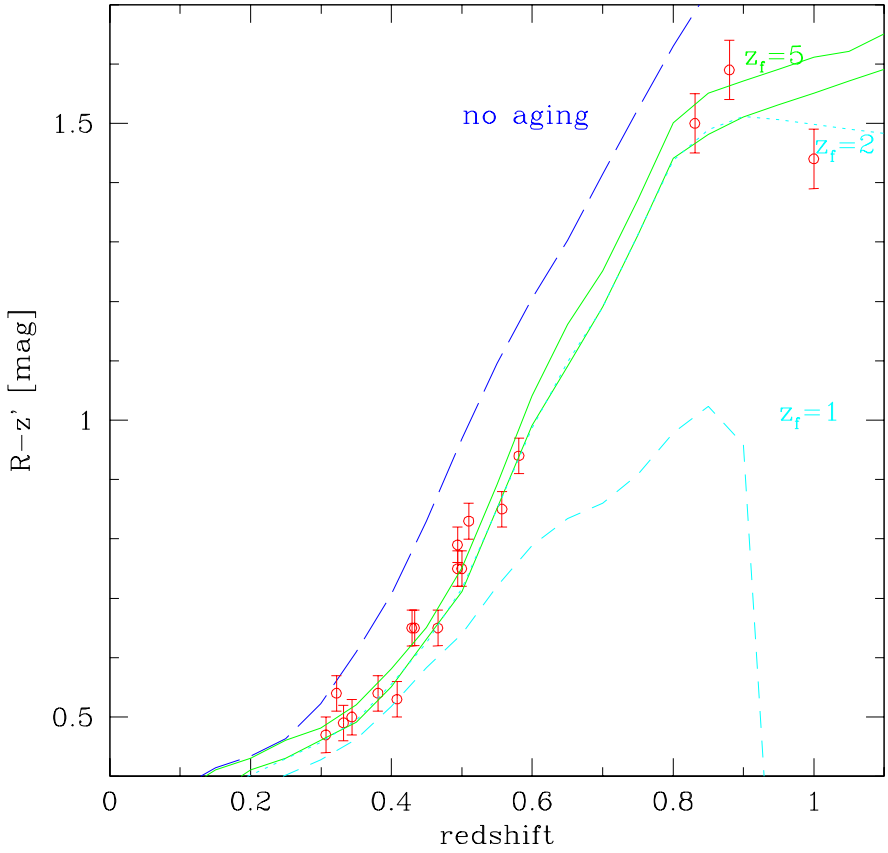

Figure 4. Observed $R-z'$ colour of the red envelope of the red sequence observed in each cluster as a function of redshift. Three galaxy evolution models are considered: a non–evolving early–type galaxy of present–day age at all redshifts, and two evolving early–type galaxy models, each characterised by a different formation redshift and mass. See text for details.

than X–ray observations. A more complete investigation of the bivariate distribution of optical and X–ray properties of distant clusters await a larger sample.

3.3 Colour evolution of the red sequence

The evolution of the color of the red sequence, as computed from the median colour of the three brightest galaxies on the red sequence (Figure 2) is displayed in Figure 4[3]. The colour error on each data point is estimated to be 0.03 mag, based upon the present estimate of the maximal variation of the photometric (flux) calibration across the camera field of view (Section 2). The three highest redshift clusters are assumed to exhibit a colour error 0.05 mag, due to the lower signal–to–noise ratio of the photometry.

The colour of the red envelope becomes monotonically redder with increasing redshift (to at least redshifts $z \sim 1$). Several model predictions are indicated in Figure 4: the top (long dashed) curve neglects aging of the stellar population. It is computed assuming a non–evolving 12 Gyr old early–type galaxy SED produced using the GISSEL98 spectral library (Bruzual & Charlot 1993). Galaxy colours are computed by convolving the spectrum with the appropriate filter transmission function together with the atmospheric transmission spectrum. Colours are zero–pointed to match the colour of early–type galaxies within the Coma cluster – the models of Kodama & Arimoto (1997) are employed for this purpose to avoid uncertainties due to the differences between the filters employed in this paper and those used for Coma galaxies by Bower, Lucey & Ellis (1992).

The data points are clearly inconsistent with a universe where the oldest stars have the same age at all redshifts, as already shown by Kodama et al. (1998). The additional models indicated in Figure 4 are more physically motivated. Passive stellar ageing and chemical evolution are incorporated employing the model of Kodama & Arimoto (1997), that assumes a formation redshift, z_f, and a total stellar mass. The two solid green curves indicate $z_f = 5$ and a total stellar mass of $\sim 1.7 \times 10^{11} M_\odot$ and $\sim 6.4 \times 10^{10} M_\odot$. The expectation for a mass of $\sim 6.4 \times 10^{10} M_\odot$ and two lower formation redshifts ($z_f = 2$ and $z_f = 1$) are plotted as dotted and short dashed curves respectively.

The colour of the envelope of the red sequence is reproduced well by models where the oldest stars form at $2 \lesssim z \lesssim 5$, in good agreement with the findings of Stanford et al. (1998) and Kodama et al. (1998) based on a set of richer clusters located within a comparable redshift range, and with Andreon et al. (2003a,b) for a sample of low redshift clusters of low optical richness, and also with Aragon–Salamanca et al. (1993) for a near–infrared study.

[3] The data points are available in electronic form at the URL http://www.brera.mi.astro.it/∼andreon/XIDindex.html

No clusters within the sample, particularly in the redshift range $0.3 < z < 0.6$ where the colour–magnitude relation is well–sampled by the observations, displays a significant deviation (i.e. $\Delta(R - z') > 0.1$) from the average trend, i.e. no cluster displays an unusually red or blue colour–magnitude relation for its redshift. This observation is similar to that noted at $z < 0.34$ in a sample of more than 150 clusters (Andreon 2003a,b).

The high formation redshift for red sequence galaxies (alternatively, the old age of the constituent stellar populations), although similar to previous studies, displays a number of important new aspects. Firstly, the observations presented form a very homogeneous data set: all clusters (with the exception of XLSSC 006) were observed with the same instrument and filters during a single observing run (XLSSC 006 was observed using the same instrument on the previous run). By way of comparison, the cluster samples presented by Stanford et al. (1998) and Kodama et al. (1998) employ a combination of telescopes and photometric passbands. Secondly, the cluster sample is mostly X–ray selected. The cluster sample is therefore selected in a manner which is independent of (or assumed to be) optical properties and avoids a potentially circular analysis between optically selected clusters and the properties of the red sequence. Thirdly, many of the clusters at $0.3 < z < 0.6$ presented within this paper display X–ray luminosities (and richness, see section 3.4) indicative of low mass or low richness clusters and groups rather than optically rich, massive clusters considered in previous studies (though c.f. Andreon 2003a,b). Low mass structures represent environments with current predictions regarding the assembly of bright, red galaxies (e.g. Kauffmann 1996 and Eggen, Lynden-Bell & Sandage 1962) are deemed to display the greatest divergence.

We note that the formation redshift computed for the sample depends in a non–trivial manner upon the assumed stellar population model: adopting a Bruzual & Charlot (1993, updated to GISSEL96) model of solar metallicity, a Salpeter IMF and a star formation e–folding time scale $\tau = 1$ Gyr, causes the formation redshift that reproduces the colour of the red sequence of the cluster sample to shift from redshifts $2 \lesssim z_f \lesssim 5$ to $z_f \sim 11$. Stanford et al. (1998) employed GISSEL96 and reported formation redshifts for early–type galaxies located on the red sequence of $2 \lesssim z_f \lesssim 5$. It is important to note that differences in the cosmological model assumed in this paper and that adopted by both Kodama et al. (1998) and Stanford et al. (1998) mean that the formation redshifts computed by these authors should be lowered somewhat when compared to the current results.

The presence of colour gradients within cluster galaxies is not expected to alter the conclusions regarding the colour evolution of the red cluster galaxy population. This assumption holds even in the current situation where the fixed angular aperture employed to measure cluster galaxy colours corresponds to a varying rest–frame aperture projected at the redshift of each cluster. There are several reasons for this expectation: 1) differential colour gradients, $\partial(B-R)/\partial \log r$, are small (e.g. 0.02 mag per decade in radius, Vader et al. 1988), and the resulting integrated colour gradient $\partial(B - R)(< r)/\partial \log r$ displays an even smaller dependence upon radius, 2) the applied angular aperture changes by a factor 2 (1/5 of a decade) in the galaxy rest–frame as the galaxy is moved from $z = 0.3$ to $z = 1.0$ and 3) the aperture is intrinsically large compared to the visible galaxy extent at all redshifts considered in the sample (about 30 kpc once seeing effects are considered – see also Kodama et al. 1988).

3.4 Cluster luminosity functions

The cluster LF is computed employing standard techniques (e.g. Oemler 1974), i.e. galaxy counts are compiled from the cluster field and a background galaxy count computed from a control field, suitably normalized to the cluster area, is subtracted. The effective cluster area is further corrected for the crowding effect due to bright stars where required (e.g. for Cl0412). Errors on the LF data points take into account the increased variance in galaxy counts due to large scale structure variations and follow the Huang et al. (1997) approach. We note that several literature papers do not take such sources of variance into account, and assume Poissonian uncertainties alone. Taking such additional sources of uncertainty into account can give rise to the misleading impression of a lower data quality when compared to quoted uncertainties for literature LFs. For example, Barrientos & Lilly (2003) do not include a term associated with large–scale structure variation in the LF uncertainty. As emphasized by Andreon & Cuillandre (2002), background fluctuations enter into the error budget twice – one contribution from the control field and one from the cluster direction field.

A single Mosaic II pointing contributing to the CTIO Rz' data set covers a field of 0.36 deg^2. For clusters located within a given CTIO pointing, we employ the area of each pointing not associated with the particular cluster detection (typically 0.33 deg^2) as the control field. The cluster area itself is a circle of radius identical to that applied to determine the colour–magnitude relation and the colour histogram (typically 2 arcminutes radius) as detailed in Section 3.1.

For clusters observed with VLT/FORS2, a circular aperture of 2 arcminute radius is applied to study the LF. Three exceptions are clusters XLSSC 002, XLSSC 003 and XLSSC 004, for which the adopted radius is 1.5 arcminutes. The choice of the control field for clusters studied employing the VLT data is more complex than the CTIO case. At redshifts $z > 0.6$ the apparent angular extent of the cluster is small and the projected cluster galaxy surface density expected at 2.5 arcminutes from the cluster centre is assumed to be negligible. Therefore, for such distant clusters, the area contained within a circular annulus of radius 2.5 to 3 arcminutes is used as a control field. At redshifts $z < 0.6$ the apparent angular extent of typical clusters contaminate most of the FORS2 field of view, making the definition of any cluster–free control area within the field impossible. For clusters located at redshifts $z < 0.6$, we employ the FORS2 field of cluster XLSSC 005 (located at $z = 1$) as the control field. The decision is motivated by the fact that the brightest member galaxy of XLSSC 005 is fainter than the faintest luminosity bin of clusters located at redshifts $z \sim 0.3$, i.e. XLSSC 005 is too distant to affect the background count level at the magnitudes sampled in lower redshift clusters. For clusters located at redshifts $z \sim 0.5$, only the faintest magnitude bin is affected by any contribution from the $z = 1$

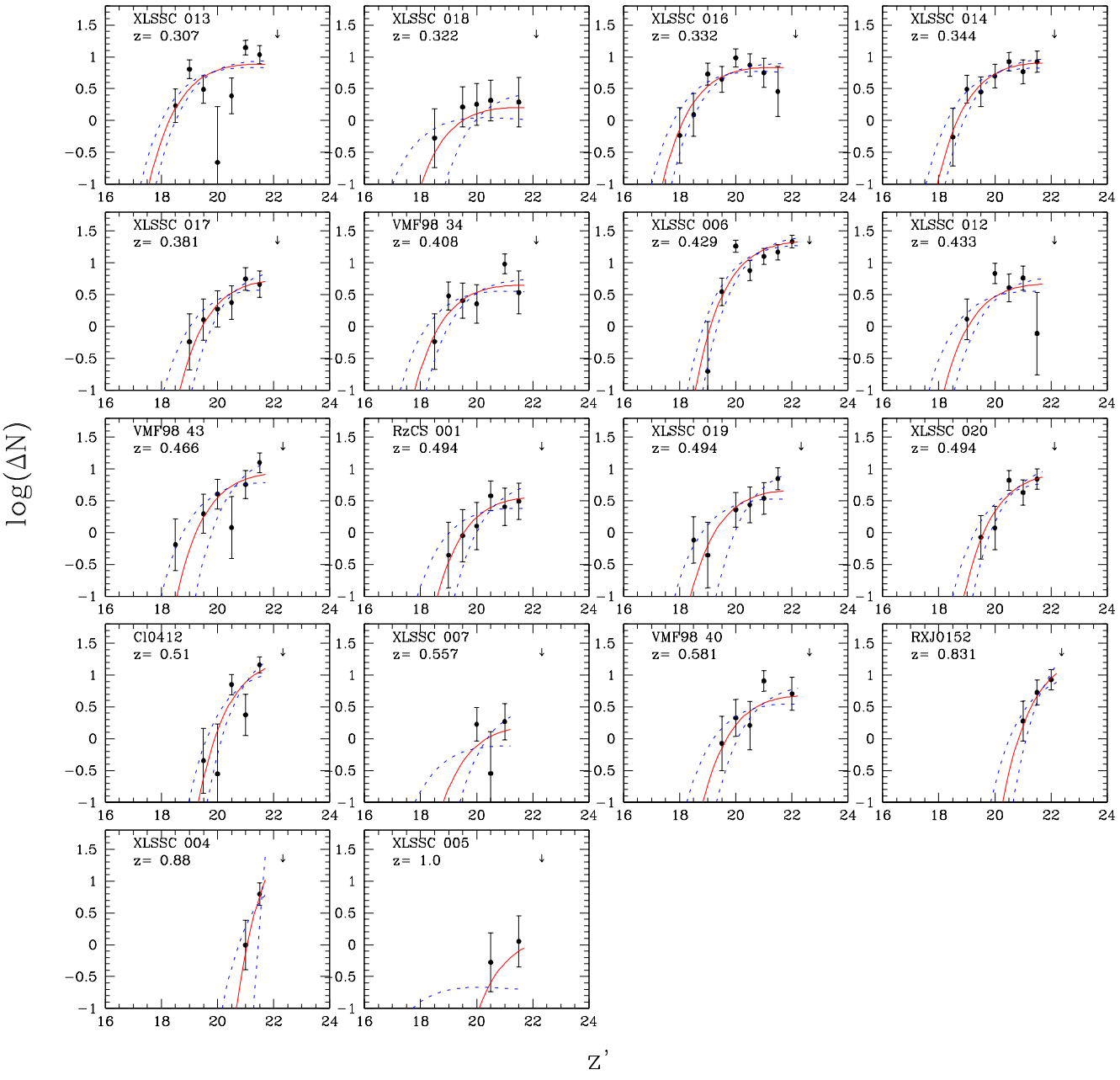

Figure 5. Cluster galaxy luminosity functions computed in the z' band. The ordinate is the logarithm of the number of galaxies per bin. The arrow marks the magnitude completeness limit. The red (solid) curve marks the best fit Schechter function, while the blue (dashed) curve marks the best fit $\pm 1\sigma$.

cluster. As an additional test, we also use a FORS2 image taken as part of the same data set of the field of a redshift $z \sim 1.3$ cluster candidate to compute the background count level. In this case there is little doubt that the distant cluster LF will not bias the computation of the background level for $z \sim 0.5$ clusters. Comparison of the $z < 0.6$ cluster LFs computed using the above two background count models indicates no significant differences.

Clusters and control fields are at most located within 1 degree of each other (for VLT data), and the majority display separations of the order of a few arcminutes. Paolillo et al. (2001) demonstrated that the only effect of selecting a background region too close to the cluster is to reduce the S/N ratio of the resulting cluster LF, without otherwise altering the resulting m^* parameter.

The LF computation employs a parametric form described by a Schechter (1976) function

$$\phi(m) = \phi^* 10^{0.4(\alpha+1)(m^*-m)} e^{-10^{0.4(m^*-m)}}, \quad (1)$$

where m^* and α are the characteristic magnitude and the slope of the LF at faint magnitude respectively. The LF normalization, ϕ^*, is not constrained in the fitting procedure. The value of the faint–end slope of the Schechter function fitted to the data is fixed at $\alpha = -0.87$ (the value derived at

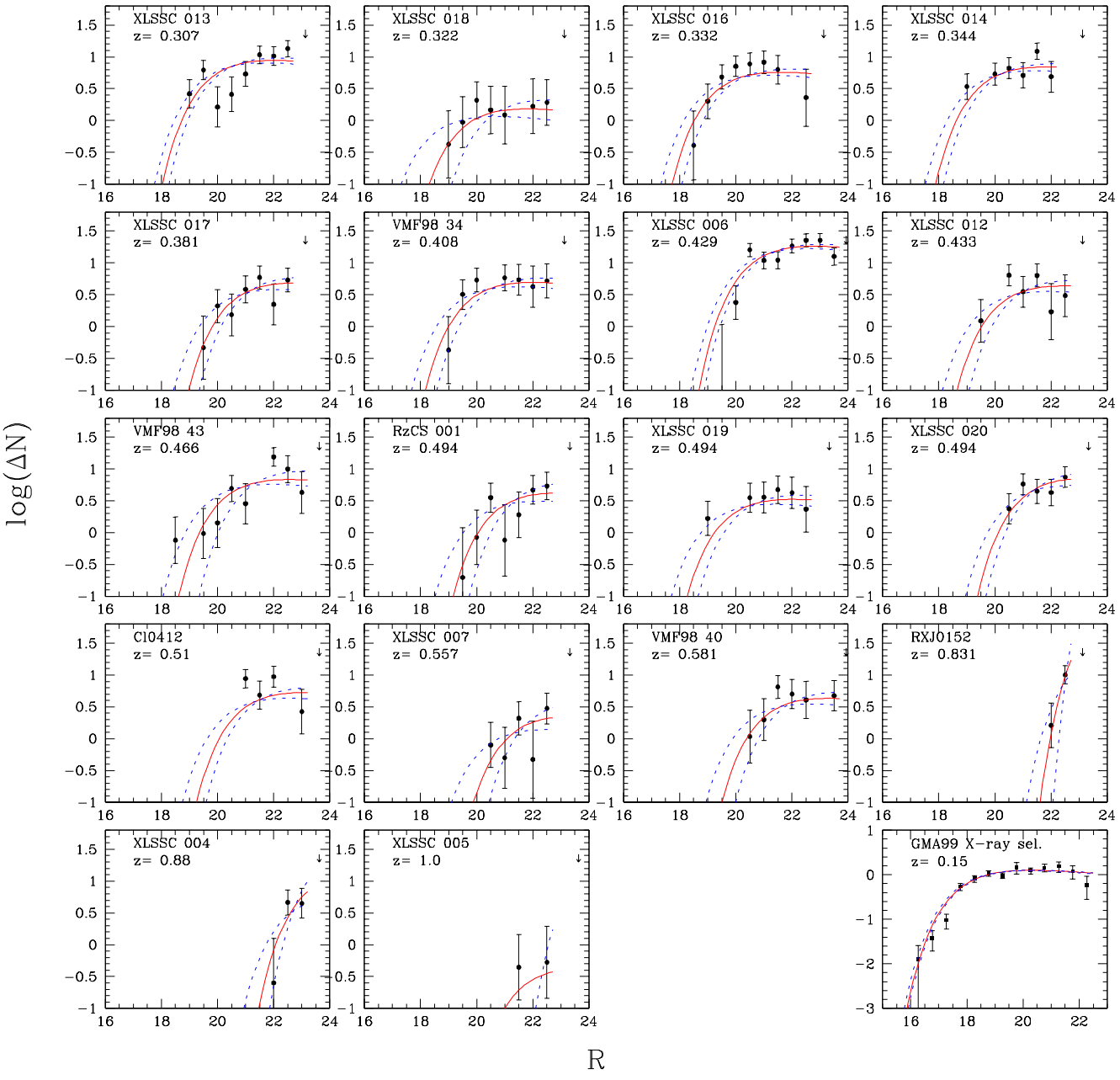

Figure 6. Cluster galaxy luminosity functions computed in the R band. Axis, symbols and curves as in previous figure. The bottom–right panel shows the low redshift R band LF of a composite sample of 21 X–ray selected clusters.

low redshift by GMA99). The slope is fixed as it is relatively unconstrained at high redshift and, as m^* and α are highly correlated, performing an unconstrained fit with respect to α will seriously undermine any constraints placed upon m^*. This approach introduces the drawback that any differential luminosity evolution occurring between bright and faint galaxies within a given cluster will be ignored (Andreon 2004). We further specify that the integral of the model LF over the observed magnitude range be equal to the observed number of galaxies, leaving m^* as the only free parameter. We also take into account the finite width of magnitude bins by convolving the model function with a rectangular window function of 0.5 mag width.

The χ^2 statistic is computed as

$$\chi^2 = \sum_{bins} (Model - Observations)^2 / error^2, \quad (2)$$

where $error^2$ is the quadrature sum of the Poisson uncertainty of the $Model$ and background contributions. We adopt a theoretical definition of χ^2 in order to include the information in magnitude bins containing no galaxies. Errors on m^* corresponding to 68% confidence levels are computed from $\chi^2 = \chi^2_{best} + 1$ (Avni 1976; Press, Flannery, & Teukolsky 1986).

The LFs presented in this paper are computed employing a specific metric aperture to determine galaxy magni-

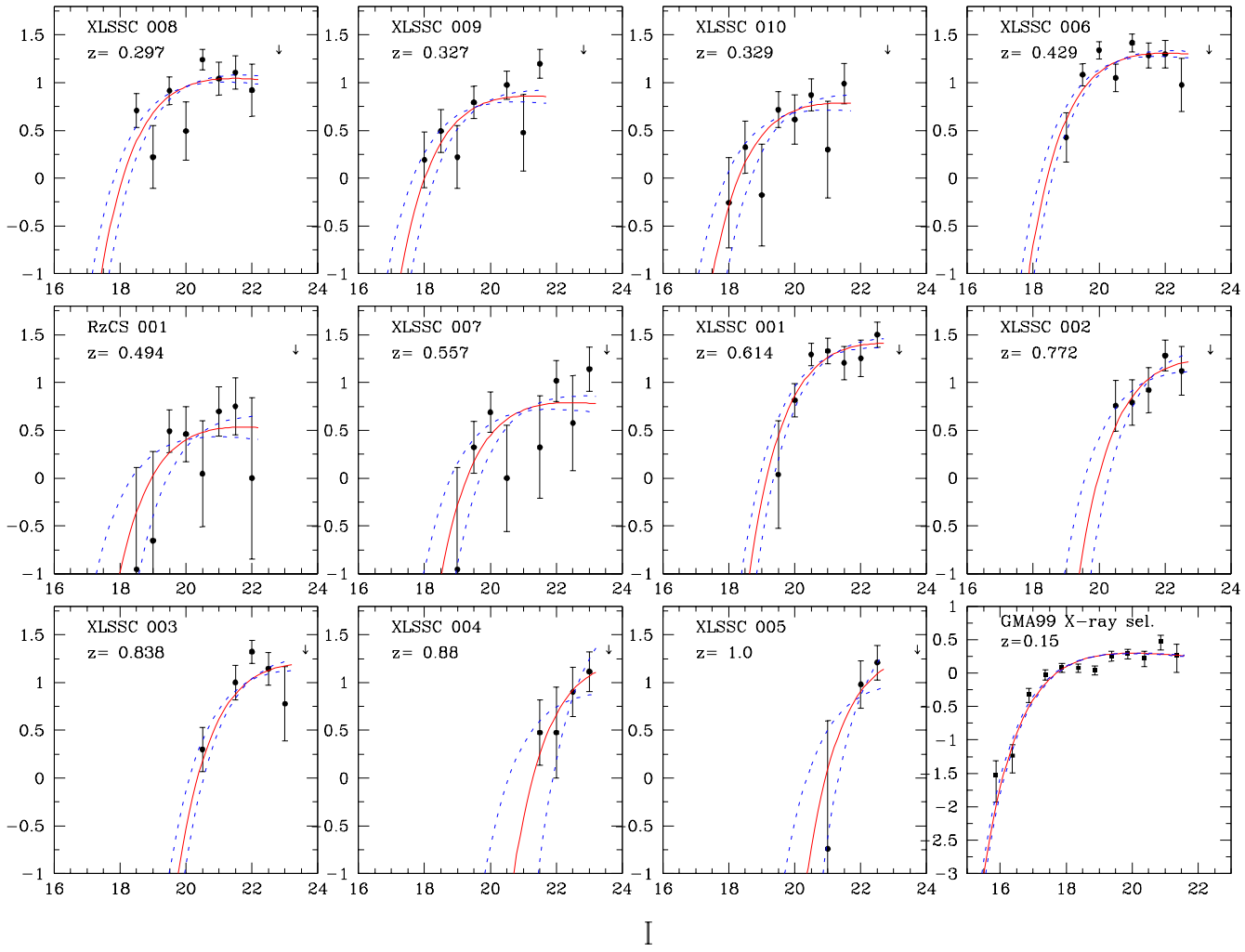

Figure 7. Cluster galaxy luminosity functions computed in the I band. Axis, symbols, curves, and low redshift sample (bottom–right panel) as in previous figure.

tudes (Section 2). The application of a metric aperture permits a consistent comparison to be made between the LFs computed at different redshifts. However, the LFs presented in this paper are not comparable to LFs computed using different photometric apertures, e.g. isophotal or pseudo–total photometric measures (as discussed in Section 2).

3.4.1 R– and z′–band LFs

Computation of the LF for high–redshift clusters is dependent upon additional cluster member selection techniques (i.e. colour selection of the red sequence) as the cluster contribution is sometime numerically small compared to the galaxy "background". Therefore, cluster R– and z'–band LFs are computed applying a selection in colour space, i.e. selecting photometric cluster members within a specific colour interval. The applied interval (with exceptions mentioned below) was 0.65 mag in $R - z'$ delimited on the red side by the colour of the red sequence plus 0.05 mag – to account for the broadening of the colour–magnitude relation by photometric uncertainties. The applied colour interval is indicated in Figure 3 by vertical arrows and in Figure 2 by horizontal lines (note that the red selection limit is redder than the red sequence marked in each figure by 0.05 mag – as outlined above). Rejecting galaxies redder than the red envelope cut–off removes galaxies that are too red to be plausibly located at the cluster redshift. No overdensity of galaxies redder than the applied colour limit is observed within any of the cluster fields (see Figure 3), except where a background cluster is located along the line of sight, e.g. XLSSC 017. Fukugita et al. (1995) indicate that the applied blue selection limit excludes galaxies bluer than "Irregular–type" at redshifts $z > 0.5$ and excludes no galaxy types at lower redshift.

The blue colour limit includes the colour range covered by the observed galaxy overdensity and no statistically significant galaxy overdensity is detected blueward of the blue colour limit for the majority of the clusters presented in this sample. Two exceptions are XLSSC 020, where XLSSC 017 is located in the foreground, and XLSSC 007, which is not detected as a significant optical overdensity and for which the colour selection interval is reduced to exclude spectroscopically confirmed interloping galaxies.

The spectroscopic galaxy sample permits an indepen-

dent check that the applied colour selection criteria do not introduce a significant level of incompleteness into the cluster galaxy sample. We found that the applied colour selection interval excludes on average only 10% of spectroscopic cluster members. This figure drops to 5% if the cluster XLSSC 007, which was assigned a smaller colour interval due an unusual background, is excluded. Therefore, the applied colour selection criteria do not exclude an important population of potential cluster members and the procedure does not bias the computation of the R– and z'–band LF. As a final test, the R– and z'–band LFs for each cluster computed without applying colour selection are compared to the LFs generated by the colour selected cluster galaxy sample.

Figures 5 and 6 display the z'– and R–band LFs for each cluster. The LFs are computed applying the above colour selection criteria. If colour criteria are not applied, statistically identical results are obtained for all but the two highest redshift clusters in the sample, plus clusters XLSSC 007 and XLSSC 020 – not unexpected given the above discussion. The limiting magnitude sampled in each cluster LF is $m < m^* + 3$ in z' and $m < m^* + 4$ in R for low redshift clusters decreasing to $m < m^*$ for high redshift clusters. The plots indicate the best fitting Schechter model (solid red line) and the models corresponding to a $\pm 1\sigma$ variation in m^* (dashed blue line). In each case a Schechter function provides an acceptable representation of the LF data at the 99 % confidence level or greater. All R– and z'–band LFs display a shift to fainter apparent magnitudes with increasing redshift (as expected). Certain clusters require additional comments:

(i) XLSSC 018 is an intrinsically poor cluster. We count only 8 galaxies brighter than the z'–band limiting magnitude within 2 arcminutes of the cluster centre. Several spectroscopically confirmed members are located outside this radius (a total of 12 galaxies have been confirmed spectroscopically as being members of this cluster).

(ii) XLSSC 006 is one of the optically richest clusters in the sample, with more than 77 photometric members within the 2 arcminute radius aperture and brighter than the z'–band magnitude limit. By counting the galaxies within the interval m_3 to $m_3 + 2$, and accounting approximately for the population outwith the nominal cluster radius, the cluster displays an Abell (1957) richness class of 0. The other clusters in the sample at similar or lower redshift display lower optical richness values. The aberrant z' LF data point at $z' = 20.0$ is deviant from the Schechter LF by several sigma, and it is therefore it is rejected from the χ^2 fitting. No other points are similarly aberrant in any of the presented clusters, and no other LF data point is rejected.

The lower–right panel of Figure 6 displays the LF computed for 21 X–ray selected clusters at redshifts $z < 0.25$ (GMA99). The transformation from the r'–band employed by GMA99 and the R–band employed for the current sample is performed by applying $R - r'$ values following Fukugita et al. (1995). One third of the GMA99 sample is X–ray selected, while half of the remaining sample is composed of clusters subsequently detected in the Rosat All Sky Survey[4]. The R–band LF derived using the GMA99 sample of 65 clusters is identical within the errors to the subset of 21 X–ray selected GMA99 clusters.

At the median redshift of the sample, $\langle z \rangle = 0.47$, the R–band samples rest–frame wavelengths $\lambda \sim 4000$ Å, whereas the z' band samples the rest–frame V–band. At such redshifts, the relative magnitude change arising from recent or continuing star formation will be greater than at rest–frame wavelengths $1.4 \lesssim \lambda(\mu m) \lesssim 1.6$ sampled by NIR (K–band) passbands.

3.4.2 I–band LF

Figure 7 displays the I–band LFs computed for the cluster sample. In contrast to the R– and z'–band LFs discussed in previous sections, no colour selection was applied to generate the I–band LF sample, either because no Rz' data was available, or, in the case of clusters common to both data sets, because of large differences in the field size between filters.

The lower–right panel displays the composite LF computed for 21 X–ray selected clusters at $z < 0.25$ (GMA99), converted from i to I using Fukugita et al. (1995), whereas the other panels show the LFs computed for individual clusters presented in this paper. The curves show the best fitting Schechter model (solid red line) and models corresponding to a $\pm 1\sigma$ variation in the m^* (dashed blue line). The Schechter function provides an acceptable fit to the LF data points at the 99 % confidence level. The limiting magnitude sampled in each cluster LF runs from $m < m^* + 3$ at low redshift to $m < m^* + 1$ at the highest redshift in the sample.

3.5 Global luminosity evolution

Values of m^* and corresponding uncertainties computed for cluster LFs in each of the three filters considered are available in electronic form [5]. LF parameters for the composite LF of the GMA99 redshift $z = 0.15$ sample are also tabulated.

Figure 8 displays the redshift dependence of 47 m^* values generated by LF computations for clusters in our sample, plus two $z = 0.15$ reference points (from GMA99), each one being the average of 21 X–ray selected clusters. To highlight the possible effects of active luminosity evolution upon m^*, the distance modulus and passive luminosity evolution terms were removed assuming a passively evolving stellar population formed at $z_f = 5$ using the model of Kodama & Arimoto (1997) – the model previously employed to compute the colour of the red sequence. The model predictions are normalized to the observed m^* at $z = 0.15$ in R and I. A local determination of the z'–band cluster LF is not currently available. We therefore adopt the computed I^* value for the local cluster sample and applied $I - z' = 0.2$ mag (Fukugita et al. 1995). The measured R–, z'– and I–band m^* values, once passive evolution has been accounted for, do not differ systematically from each other – further confirmation that the colour selection applied to compute the

[4] This is demonstrated by comparing the GMA99 and Cruddace et al. (2002) cluster lists.

[5] at the URL http://www.brera.mi.astro.it/∼andreon/XIDindex.html

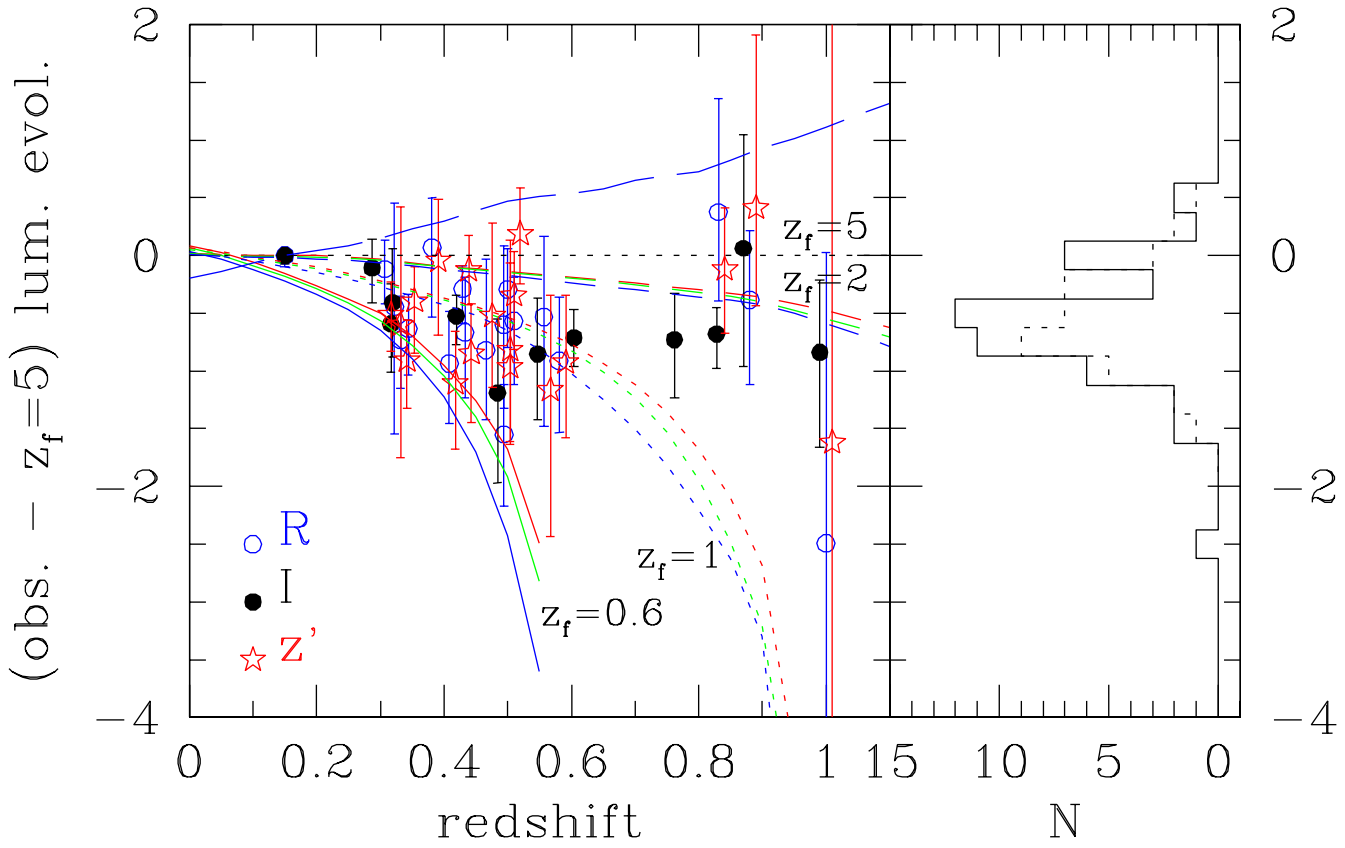

Figure 8. *Left panel:* Characteristic LF magnitude, m^*, evolution as a function of redshift having removed the contribution from passive ($z_f = 5$) stellar evolution, and from luminosity distance. The labelled curves are the predictions for different formation redshifts. Points and curves of the same colour refer to the same filter, as indicated within the figure. The long–dashed curve is the R–band expectation neglecting stellar evolution. Points are slightly offset in redshift in order to limit crowding. The R and I calibrating points at $z = 0.15$ (mean of 21 clusters) fall one on the top of the other and hence are not easily to see separately. *Right panel:* frequency distribution of the points in the left panel (solid histogram) and of the corresponding values derived without any colour selection and excluding problematic clusters.

R– and z'–band LFs, but not employed for the I–band, has little impact on the computed value of m^*.

The m^* data points are systematically brighter than a model based upon an old, passively evolving stellar population (the horizontal dashed line in Figure 8). A non–evolving model is also strongly ruled out. The clusters presented in Figure 8 require the occurrence of a secondary star formation episode at lower redshift than the $z_f = 5$ in order to generate m^* values brighter than the passive evolution model. The same conclusion can be drawn by considering the right panel of Figure 8 (solid line) which displays the histogramme of m^* values summed over redshift. The resulting m^* distribution is approximately 1 magnitude wide and is offset from zero. The dotted histogramme in the same panel displays the m^* histogramme computed for cluster LFs generated without colour selection and by rejecting problematic clusters (i.e. clusters blended along the line of sight and those displaying m^* errors larger than 0.6 mag), demonstrating again that the applied colour selection does not introduce a significant bias.

Paolillo et al. (2001) and Andreon (2004) demonstrate that the LF shape computed for galaxies drawn from extended cluster regions are statistically equal to the corresponding LF shape computed for galaxies drawn only from the central cluster regions. Therefore, the specific choice of cluster aperture radius employed to generate the cluster LF sample should not introduce a significant bias into the resulting LF computation. GMA99 and Paolillo et al. (2001), both show that the slope of the composite LF of many clusters, in the magnitude range sample in these works and in the present paper, does not depend on wavelength from g, or B_j, to i. Christlein, McIntosh & Zabludoff (2004) shows the similarity of the slopes in the U and R bands of the composite LF of three clusters. Therefore, our results should not be biased by a wavelength–dependent slope. A remaining concern may be that the reference m^* value at low redshift (i.e. the GMA99 data) could be inappropriate for the current sample of (typically) low richness clusters, as the GMA99 sample includes some optically richer clusters. The right panel of Figure 8 indicates that, in order to remove the supposed luminosity evolution, m^* should depend on optical richness as much as 1 mag when considered across the range of richness values displayed by clusters in the current sample. Within the large GMA99 sample there is a 0.01 ± 0.15 mag difference in m^* between rich and poor clusters. This indicates that, while the m^* normalization as a function of

richness may play some role, it is unlikely to account for the apparent evolution in m^* with redshift.

The additional curves in Figure 8 indicate the expected m^* evolution for stellar populations formed at successively lower redshifts. In order to account for the bright m^* values observed at redshifts $z \sim 0.3$ a formation redshift as low as $z_f = 0.6$ would be required, although, by adopting such a low formation redshift, the predicted m^* value at a redshift $z = 0.15$ would be 0.2 magnitudes brighter than that reported by GMA99. The LF data points are not well described by any formation model based upon a single episode of star formation and at least two important star formation events are required. The last (in cosmic time) star formation event should brighten average m^* values by up to 1 magnitude (right panel of Figure 8). Such secondary star formation activity may be related to the Butcher–Oemler effect (Butcher & Oemler 1984), although the evidence for the latter is not compelling (Andreon & Ettori 1999; Andreon, Lobo & Iovino 2004). A Butcher–Oemler analysis of the present sample of clusters is presently in progress.

A similar study by de Propris et al. (1999), performed for optically rich clusters in the K–band, reported a redshift evolution of m^* consistent with the prediction of a passively evolving stellar population. In contrast, the current data set appears to indicate that a secondary star formation episode is required. However, for clusters considered to redshifts $z < 1$, the K–band samples the rest–frame contribution of old stars when weighted by luminosity. The secondary star formation episodes supported by the current data set compiled with red optical (rest–frame blue) passbands would not result in a strong signal in the K–band cluster LF evolution. We note also that a large dispersion is present in the m^* values presented by de Propris et al. (1999), and that several data points are brighter by 2 σ than a prediction considering a passively evolving stellar population formed at a redshift $z_f = 3$. There is therefore no contradiction between the de Propris et al. (1999) LF evolution and the results on luminosity evolution in clusters presented in the current paper.

The sample of cluster LF m^* values presented in this study are not consistent with the prediction of a single evolutionary model, in qualitative agreement with Dahlén, Fransson, Östlin, & Näslund (2004). Therefore, not all clusters share the same evolutionary history, for example because composed of different proportions of passive and active evolving galaxies, leading to a distribution of LF properties. Under such circumstances the computation of a composite LF for a sample of cluster would be of questionable merit. Compilation of a large sample of clusters to redshifts up to $z \sim 1$ according to well–defined criteria will permit a detailed investigation of the galaxy cluster LF and sources of dispersion therein. This aim represents one of the scientific goals of the continuing XMM–LSS survey.

3.6 Comparison with previous works

3.6.1 Barrientos & Lilly (2003)

Barrientos & Lilly (2003, hereafter BL03) present a study of the luminosity and colour properties of 8 galaxy clusters located within the redshift interval $0.40 < z < 0.48$. The authors present I–band cluster LFs and a composite $V - I$ colour magnitude diagram. One of the central claims of their paper is that the characteristic magnitude m^* of the cluster LF evolves passively – a conclusion apparently at variance with that presented in this work. Specifically, comparison of the BL03 and our LF analysis indicates an offset in the characteristic magnitudes evolution at the level of 0.5 magnitudes for the two cluster samples drawn from an overlapping redshift interval. This section addresses the causes of this discrepancy. BL03 reported a best fitting characteristic magnitude of $I^* \sim 19.3$ for red cluster galaxies, generally in good agreement with values computed in the current paper of $I^* = 19.2$ at $z = 0.33$ to $I^* = 19.6$ at $z = 0.42 - 0.49$. However, one should note that the computation presented in the current paper includes galaxies of all colour, and that the two samples employ marginally different faint–end slopes.

In order to constrain the brightness evolution of the LF, BL03 convert apparent I^* values to rest–frame, absolute M_V values assuming a cosmological model described by the parameters $q_0 = 0.5$ or 0.1 and $\Omega_\Lambda = 0$. When compared to the cosmological model considered in this work (and supported by current observations), the BL03 assumed model results in galaxies appearing fainter by 0.37 or 0.18 magnitudes respectively, than in our cosmological model.

In addition, to convert from observed I to rest–frame V magnitudes, BL03 employ the $V - I$ colour of a present day elliptical galaxy. Figure 4 indicates that the reddest galaxies at $z = 0.4$ are 0.2 magnitudes bluer in $R - z'$ compared to a present day elliptical galaxy. Kodama et al. (1998) show that the same holds true in the $V - I$ colour. Hence, the $V - I$ colour assumed by BL03 is 0.2 mag too red.

Therefore, in computing absolute M_V values from apparent I–band magnitudes observed for elliptical galaxies at typical redshifts $z \sim 0.45$, BL03 introduce a total systematic offset of $0.2 + (0.37, 0.18)$ magnitudes in the sense that their final M_V values for galaxies at $z \sim 0.4$ are fainter than values computed employing observed colours at $z \sim 0.45$ and a Λ dominated universe.

In order to constrain the amplitude of luminosity evolution from a redshift $z \sim 0.45$ to $z = 0$, BL03 employ a sample of low–redshift clusters compiled by Lopez-Cruz (2001). Formation of a consistent comparison is hindered by the fact the LF parameters for the Lopez-Cruz (2001) sample are computed independent of cluster galaxy colour (recalling that the BL03 sample is restricted to colour–selected early–type galaxies) in addition to the requirement to apply further corrections to account for the different photometric filter response functions. Most importantly, the median redshift of the Lopez-Cruz (2001) cluster sample is $z \sim 0.1$. However, the "local" ($z = 0$) LF parameters derived from Lopez-Cruz (2001) neglect the effects of passive stellar evolution from $z = 0.1$ to $z = 0$. In simple terms, Lopez-Cruz (2001) measures m^* at $z = 0.1$ (a general discussion can be found in Andreon 2004). The passive evolution expectation should be, therefore, computed from $z_{low} = 0.1$ to $z_{high} \sim 0.45$, whereas BL03 take $z_{low} = 0$. Because of overestimation of the redshift baseline, BL03 introduce a further magnitude offset of 0.1 magnitudes in the sense that the apparent evolution thus computed is underestimated by 0.1 magnitudes, as directly measured by Blanton et al. (2003) and Andreon (2004), and in agreement with passive evolution models (e.g. Bruzual & Charlot 1993).

We therefore conclude that BL03 underestimate the lu-

minosity evolution within their cluster sample by 0.67 to 0.48 magnitudes (with the two values generated by the two cosmological models assumed in BL03), exactly the discrepancy between the m^* evolution of the BL03 sample and the current work. Application of these corrections to the BL03 data indicates a R–band luminosity evolution amplitude of 1.4 magnitudes (with errors greater than 0.5 magnitudes) compared to an expected passive evolution amplitude of approximately 0.5 magnitudes. We conclude that the BL03 data do support an additional luminosity evolution term in excess of that expected on the basis of passive evolution alone. Based upon these arguments we claim that the 'active' luminosity evolution claimed in the current paper is observed in the BL03 sample.

3.6.2 Nelson et al. (2001).

Nelson et al. (2001; hereafter N01) compute m^* values for the I–band LF distributions of 12 clusters with spectroscopic redshifts in the range $0.35 < z < 0.65$ (see their Table 2). Comparison of the cluster luminosity distributions presented in N01 with those presented here indicate that observations of the former are shallower or comparable to our ones. When the N01 sample is augmented by literature data, Nelson et al. report a variation of 1.65 magnitudes in m_I^* in the range $0.35 < z < 0.85$. The passive evolution model prediction in the same redshift range is 2.65 magnitudes, i.e. the observed characteristic magnitude is about one magnitude brighter compared to the passive expectation – in excellent agreement with our findings. However, N01 report a different conclusion, stating that m^* is evolving passively according to a stellar population formed at a redshift $z_f = 1.7$ (right–hand panel of their Figure 11), because N01 employ an older cosmological model. Their data, in the present cosmological model, are well described by the evolution of a stellar population forming at $z_f \sim 0.7$, in good agreement with our claim of a secondary (i.e. below $z < 1$) star formation activity pointed out by our data. We note that a direct comparison of LF values is not possible as a result of the particular LF fitting procedure adopted by N01.

4 DISCUSSION AND CONCLUSIONS

We have studied a sample of 24 clusters located at redshifts $0.297 < z < 1$, of which 16 display redshifts $z > 0.4$ and 6 have $z > 0.6$. The majority of the clusters are either X–ray selected or detected, and we are therefore observing gravitationally bound systems. Most of the cluster sample, particularly clusters at redshifts $z < 0.6$, possess X–ray luminosities and optical richness values typical of groups or low mass clusters.

All clusters in our sample, despite the primary X–ray selection and low X–ray flux/optical richness displayed by the majority of the sample, display a statistical overdensity of galaxies of similar colour (Figure 3), that make them detectable by an almost 3 dimensional search defined by sky position and colour. In fact, all clusters with R and z' photometry, with the exception of XLSSC 007, are colour–detected. However, the present optical identification of XLSSC 007 as the counterpart of the extended X–ray source is uncertain as a result of the large distance between the optical overdensity and X–ray centres. Should the identification of this X–ray source change to that of a $z > 1$ cluster, then no X–ray selected cluster presented in this paper is missed by the $R - z'$ technique in the $z < 1$ regime. Most of the clusters are identified in X–rays, largely independent of the optical luminosity of the member galaxies. Therefore, the colour detection is non–trivial. The majority of the clusters are optically poor (Abell richness class 0 or lower) consistent with the low computed X–ray luminosities. We have therefore demonstrated that a colour plus spatial overdensity search technique can effectively identify optically poor systems at intermediate to high redshifts (at least those previously identified in X–rays).

The emerging picture from the current study is the one of a typical cluster composed of two or more distinct galaxy populations : a relatively old population evolving passively (as measured from the evolution of the color of the red sequence) together with a younger population, ostensibly responsible for the apparent brightening of the characteristic LF magnitudes.

The reddest galaxies within each cluster/group evolve in a manner consistent with a model early–type galaxy formed between redshifts $2 \lesssim z_f \lesssim 5$ (Figure 4). This observation is largely in agreement with previous studies. We note, however, that previous studies employ cluster samples dominated by optically rich systems often observed with heterogeneous instruments. In contrast, the current study consists of an exceptionally uniform cluster sample observed under largely uniform conditions. Previous studies estimate similar values for z_f, though assuming different cosmological models, evolutionary models, or both. We note that the formation epoch of cluster galaxies estimated for the current sample would correspond to a higher redshift for the same assumptions adopted in literature.

The younger population is detected by studying the LF. The LF of each cluster has been computed in $R-, I-$ and z'–bands and is displayed in Figures 5 to 7. A Schechter function provides an acceptable description of the LF shape over the magnitude range extending from $m < m^*$ to $m < m^*+4$, with exact values depending on redshift and filter. The distribution of LF m^* values versus redshift is systematically brighter than predictions based upon a passively evolving stellar population formed at $2 \lesssim z_f \lesssim 5$ perhaps because our redshifts are sampling "the time of rapid cluster building" (Dressler 2004). The m^* values are, on average, almost one magnitude brighter than the passive evolution prediction – indicative of *active* luminosity evolution, or secondary star–formation activity. The RIz' passbands used in this study sample galaxy emission at typical rest–frame wavelengths corresponding to the $B-$ and $V-$bands. The resulting LFs are therefore more sensitive to the effects of recent star formation than cluster studies over similar redshift intervals employing NIR passbands. The evolution of m^* provides a measure of the evolution of the *whole* galaxy population, as opposed to that derived from the colours of the reddest galaxies that monitor the evolution of the oldest cluster galaxies. Overall, the galaxy population is actively evolving.

Therefore, we have detected two distinct galaxy populations, one passively evolving and another one actively evolving. The determination of the nature of this secondary activity (e.g. the time scale and the relationship with the cluster

properties and the identification of the active evolving population) is within the reach of the XMM–LSS project, since the $z < 1.3$ redshift regime will be ultimately sampled by several hundreds of X–ray selected clusters with supporting multi–colour and spectroscopic observations.

ACKNOWLEDGEMENTS

We thank T. Kodama for providing his model predictions, C. Mullis for providing galaxy redshifts in advance of publication, L. Jones, M. Paolillo for their comments to the earlier version of this papers and A. Dressler and collaborators of the XMM–LSS project for stimulating conversations. The referee is acknowledged for pointing out a literature paper initially forgot by us and for comments that improved the paper presentation. H.Q. thanks the FONDAP Centro de Astrofisica for partial support and the award of a Guggenheim Foundation fellowship. SA has received support from MURST-COFIN n. 2003020150-005.

REFERENCES

Abell, G. O. 1958, ApJS, 3, 211
Andreon, S. 1998a, A&A, 336, 98
Andreon, S. 1998b, ApJ, 501, 533
Andreon, S. 2001, ApJ, 547, 623
Andreon, S. 2003a, A&A, 409, 37
Andreon, S. 2003b, ApSS, 285, 143 (astro-ph/0304149)
Andreon, S. 2004, A&A, 416, 865
Andreon, S. & Cuillandre, J.-C. 2002, ApJ, 569, 144
Andreon, S. & Ettori, S. 1999, ApJ, 516, 647
Andreon, S., Lobo, C., Iovino A., 2004, MNRAS, 349, 889
Andreon, S. & Pelló, R. 2000, A&A, 353, 479
Andreon, S., Pelló, R., Davoust, E., Domínguez, R., & Poulain, P. 2000, A&AS, 141, 113
Aragon-Salamanca, A., Ellis, R. S., Couch, W. J., & Carter, D. 1993, MNRAS, 262, 764
Avni, Y. 1976, ApJ, 210, 642
Barrientos, L. F. & Lilly, S. J. 2003, ApJ, 596, 129
Bertin, E. & Arnouts, S. 1996, A&AS, 117, 393.
Bower, R. G., Lucey, J. R., & Ellis, R. S. 1992, MNRAS, 254, 601
Bower, R. G., Kodama, T., & Terlevich, A. 1998, MNRAS, 299, 1193
Bruzual A., G. & Charlot, S. 1993, ApJ, 405, 538
Butcher, H. & Oemler, A. 1984, ApJ, 285, 426
Couch, W. J., Ellis, R. S., MacLaren, I., & Malin, D. F. 1991, MNRAS, 249, 606
Cruddace, R. et al. 2002, ApJS, 140, 239
Dahlén, T., Fransson, C., Östlin, G., & Näslund, M. 2004, MNRAS, 350, 253
Dalcanton, J. J. 1998, ApJ, 495, 251
Donahue, M. et al. 2002, ApJ, 569, 689
de Propris, R., Stanford, S. A., Eisenhardt, P. R., Dickinson, M., & Elston, R. 1999, AJ, 118, 719
de Propris et al. 2003, MNRAS, 342, 725
de Propris, R., Stanford, S. A., Eisenhardt, P. R., Dickinson, M., & Elston, R. 1999, AJ, 118, 719
Dressler, A., 2004, in Carnegie Observatories Astrophysics Series, Vol. 3: Clusters of Galaxies: Probes of Cosmological Structure and Galaxy Evolution, ed. J. S. Mulchaey, A. Dressler, and A. Oemler (Cambridge: Cambridge Univ. Press), in press
Ebeling, H., Edge, A. C., Fabian, A. C., Allen, S. W., Crawford, C. S., & Boehringer, H. 1997, ApJL, 479, L101
Ebeling, H. et al. 2000, ApJ, 534, 133
Eggen, O. J., Lynden-Bell, D., & Sandage, A. R. 1962, ApJ, 136, 748
Ellis, R. S., Smail, I., Dressler, A., Couch, W. J., Oemler, A. J., Butcher, H., & Sharples, R. M. 1997, ApJ, 483, 582
Fukugita, M., Shimasaku, K., & Ichikawa, T. 1995, PASP, 107, 945
Garilli, B., Bottini, D., Maccagni, D., Carrasco, L., & Recillas, E. 1996, ApJS, 105, 191
Garilli, B., Maccagni, D., & Andreon, S. 1999, A&A, 342, 408
Gilbank, D. G., Bower, R. G., Castander, F. J., & Ziegler, B. L. 2004, MNRAS, 348, 551
Gladders, M. D. & Yee, H. K. C. 2000, AJ, 120, 2148
Huang, J.-S., Cowie, L. L., Gardner, J. P., Hu, E. M., Songaila, A., & Wainscoat, R. J. 1997, ApJ, 476, 12
Kauffmann, G. 1996, MNRAS, 281, 487
Kodama, T. & Arimoto, N. 1997, A&A, 320, 41
Kodama, T., Arimoto, N., Barger, A. J., & Arag'on-Salamanca, A. 1998, A&A, 33 4, 99
Landolt, A. U. 1992, AJ, 104, 340
Lopez-Cruz O., 2001, RMxAC, 11, 183
Mullis, C. R., et al. 2003, ApJ, 594, 154
Nelson, A. E., Gonzalez, A. H., Zaritsky, D., & Dalcanton, J. J. 2001, ApJ, 563, 629
Oemler, A. J. 1974, ApJ, 194, 1
Paolillo, M., Andreon, S., Longo, G., Puddu, E., Gal, R. R., Scaramella, R., Djorgovski, S. G., & de Carvalho, R. 2001, A&A, 367, 59
Pierre et al. 2003, PASP, submitted (astro-ph/0305191)
Press, W. H., Flannery, B. P., & Teukolsky, S. A. 1986, Numerical Recipes, Cambridge: University Press
Romer, A. K. et al. 2000, ApJS, 126, 209
Schechter, P. 1976, ApJ, 203, 297
Smail, I., Ellis, R. S., Dressler, A., Couch, W. J., Oemler, A. J., Sharples, R. M., & Butcher, H. 1997, ApJ, 479, 70
Smith, J. A. et al. 2002, AJ, 123, 2121
Stanford, S. A., Eisenhardt, P. R., & Dickinson, M. 1998, ApJ, 492, 461
Stoughton, C. et al. 2002, AJ, 123, 485
Trentham, N. 1997, MNRAS, 286, 133
Vader, J. P., Vigroux, L., Lachieze-Rey, M., & Souviron, J. 1988, A&A, 203, 217
Valtchanov et al. 2004, A&A, submitted (astro-ph/0305192)
Vikhlinin, A., McNamara, B. R., Forman, W., Jones, C., Quintana, H., & Hornstrup, A. 1998, ApJ, 502, 558
Willis et al. 2004, A&A, in preparation

This paper has been typeset from a TEX/ LATEX file prepared by the author.